Vol. 56, pp. 149-162, 1984

Inhaled Particles in Human Disease and Animal Models: Use of Electron Beam Instrumentation

by Arnold R. Brody*

The mineral pneumoconioses (lung disease caused by inhalation of inorganic dust) have been an important disease entity for centuries. In the last several decades, the electron microscope has been used to elucidate the distribution and identification of inhaled minerals, to aid in establishing etiologic factors, and less commonly, to determine the basic biologic mechanisms through which inhaled minerals cause lung disease. In this section, I review the instrumentation and tissue preparation currently used to address some modern problems in particle-induced lung disease. For example, human pneumoconioses of undetermined etiology can be clarified by electron microscopy and X-ray energy spectrometry. In addition, the initial deposition patterns of asbestos and silica are demonstrated in animal models, and the contributions of electron microscopy in establishing the initial lesions of asbestosis are described.

Introduction

A significant proportion of lung disease is caused by inhaling inorganic dust particles (*1*). Well-known historical examples still important today are asbestosis (*2*) and silicosis (*3*). Recent exposures to volcanic ash from eruptions of Mt. St. Helens have offered new problems and currently pose numerous questions regarding dust toxicity (*4*). Often, individuals are exposed to a mixture of particulates, and the etiology of their disease is difficult to determine (*5*). Through the past few decades, experimental animals have been used as models of these dust inhalation diseases (*3,6,7*). Both in humans and the animal models, very little is known about the basic mechanisms of particle-induced lung disease since most available information concerns the nature of particle deposition and distribution in lungs and airway models (*8*).

This chapter has two main purposes: (1) to demonstrate the utility of electron microscopy as a diagnostic tool for dust-related lung disease, and (2) to present the unique perspective which can be gained through ultrastructural studies of lung tissue from animal models of particle-induced disease.

Both in animals and man, the size and shape of airborne particles dictate the pattern of deposition in the upper airways and parenchyma of the lungs (*8,9*). This concept has been covered in detail in other segments of this book and in several reviews (*10*). In general, it has been determined that particles with a diameter greater than 20 μm will not be inhaled beyond the conducting airways. Particles with a diameter between 0.05 and 20 μm are likely to bypass the airways and deposit initially on alveolar duct surfaces and within individual alveolar spaces (Fig. 1). Particulates smaller than 0.05 μm can behave as a gas and may be exhaled before being deposited in the lung (*10*). Since particle diameter, not length, controls the deposition of inhaled materials, it is possible to find thin (diameter~0.5 μm), 50 to 100 μm long fibers within the lung parenchyma (*11*) (Fig. 2).

The many varieties of inorganic particles that cause lung disease and the natural defensive strategies mounted to clear such particles have been extensively studied and reviewed (*12–14*). The application of electron beam instruments to such studies is relatively new, however, and is considered in the following sections.

Instrumentation and Specimen Preparation

Transmission Electron Microscopy (TEM)

The conventional TEM is the original electron beam instrument used to study inorganic particles in biological material (*5*). Since the mid-1950s, TEM has been a valuable tool both for research and diagnosis. Currently, the resolving power of a modern TEM is approximately 1.5 Angstrom units; this is about 50 times the resolving

*Laboratory of Pulmonary Function and Toxicology, National Institute of Environmental Health Sciences, Research Triangle Park, NC 27709.

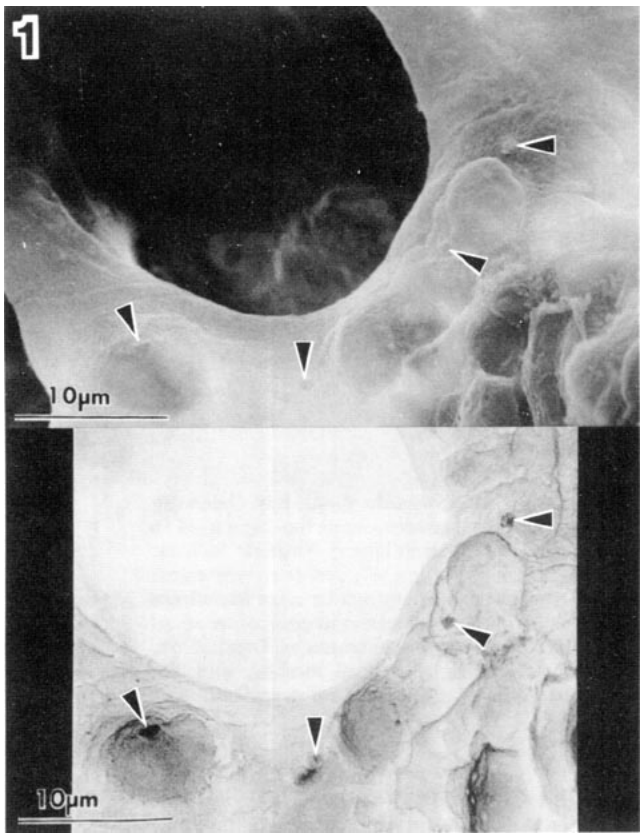

FIGURE 1. Scanning electron microscopy (SEM) (top) reveals small particles (arrowheads) of inhaled Mt. St. Helen's volcanic ash on an alveolar duct surface in the lung of a rat. Backscattered electron imaging (BEI) provides increased contrast of the individual (bottom) particles on a biological surface.

power necessary to discern the bimolecular lipid leaflet of a cell membrane. This high resolution in association with useful magnifications approaching 100,000X allows the clear observation of intracellular inclusions and accurate determination of the cell types involved (Fig. 3).

Numerous excellent sources of information on the theory and operation of electron microscopes are available (*15,16*). For our purposes here, it is sufficient to understand that the conventional TEM has as its illuminating source an electron beam produced from a tungsten or lanthanum filament. The penetrating power of the beam originates in accelerating voltages (applied to the filament) which can vary from 20 to 200 kv in modern instruments. The electron beam passes through a series of electromagnets which serve as lenses to control the diameter, magnifications and focus of the beam as it passes through the specimen (*17*). The final image of the specimen actually is a shadow cast on a phosphorescent screen by the illuminating electron beam. Thus, the more dense components of a sample will appear darker on the viewing screen. Since inorganic particles generally are quite electron-dense, TEM is particularly useful for imaging such particles both in tissue and after extraction (see below).

There are essentially two types of samples prepared for observation by TEM: embedded, thin-sectioned tissue, and particulates separated from tissue or prepared from mineral samples. Again, much information is available on tissue and particle preparation for conventional TEM (*16,18–20*). Briefly, it should be understood that if an investigator wishes to study the morphology of intracellular particles, it is necessary to follow several basic preparative steps; some of these

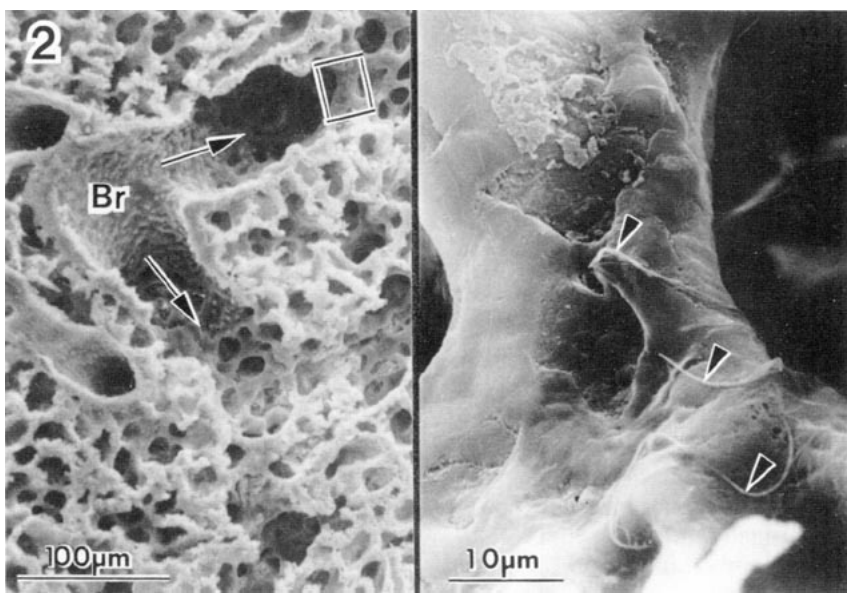

FIGURE 2. SEM demonstrates a terminal bronchiole (Br) in a rat lung and the alveolar ducts (arrows) which extend from the bronchiole. A bifurcation of two alveolar ducts is delineated and appears at higher magnification (right) to reveal several small asbestos fibrils (arrowheads) on the alveolar duct surface.

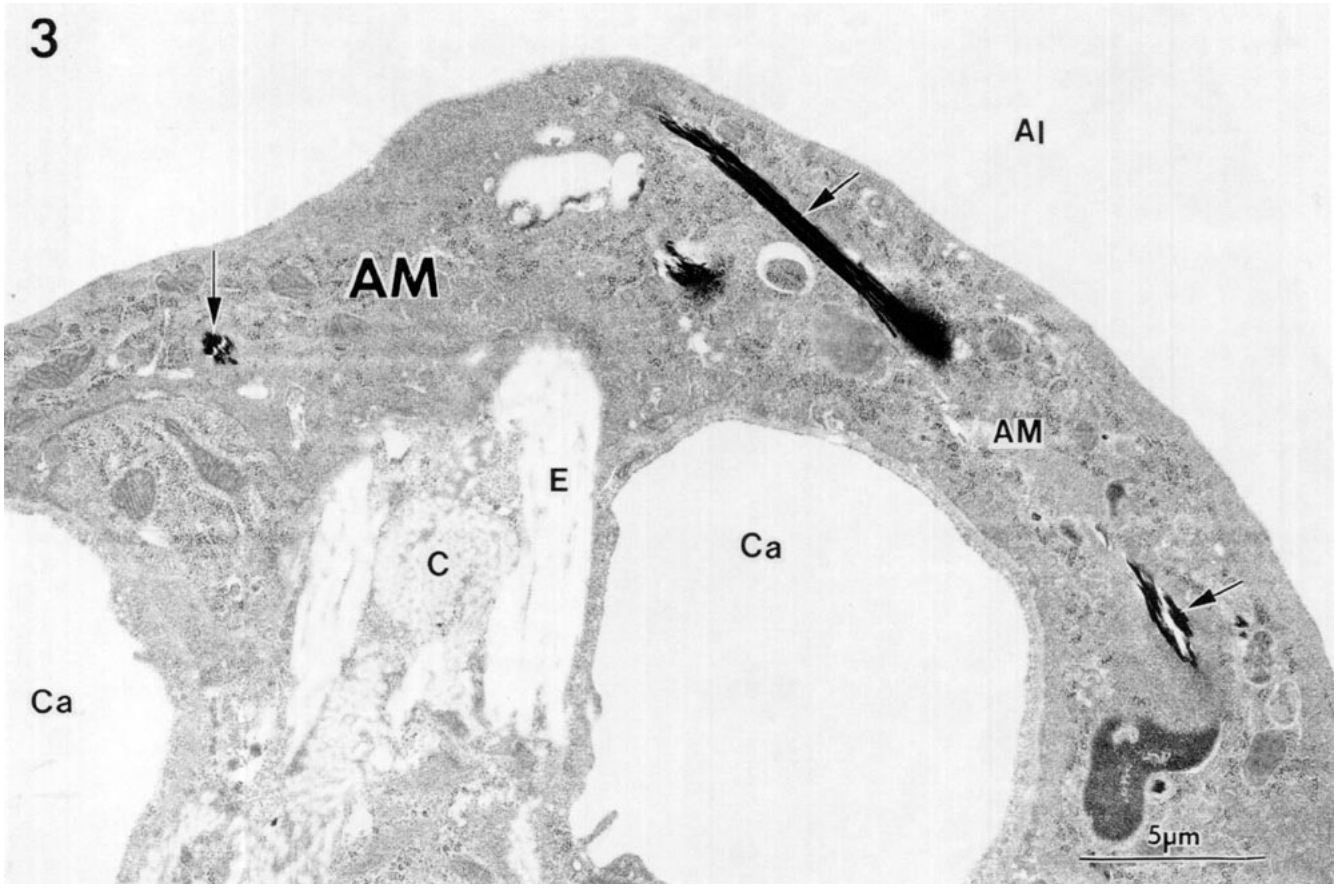

FIGURE 3. Transmission electron microscopy (TEM) shows an alveolar macrophage (AM) spread over the surface of an alveolar duct. The cell is adjacent to an alveolar space (Al) and contains chrysotile asbestos (arrows) which was inhaled several hours earlier. Underlying capillaries (Ca) and connective tissue [both collagen (C) and elastic (E)] are seen.

steps are essential for studying inorganic particles in lung tissue and are discussed below.

Tissue Fixation. Once particles have been inhaled, it is important to rapidly fix the lung tissue so particles are not displaced. This can be accomplished both in human and animal lungs by vascular perfusion with an aldehyde fixative. Increased use of Karnovsky's fixative (*21*) has shown this to be a superior solution, although glutaraldehyde still remains popular because of its excellent qualities as a fixative for electron microscopy (*16*). However, it has been shown that Karnovsky's provides best results if one wishes to carry out studies by both light and electron microscopy (*22*). Initial fixation with glutaraldehyde renders the tissue brittle and difficult to work with by conventional paraffin embedding and microtome sectioning.

Fixation by perfusion of aldehyde through the pulmonary vasculature is the method of choice for maintaining the integrity of particle distribution in the lung. Human lung tissue derived from resection or biopsy procedures can be perfused through cannulated vessels exposed on the cut surface of the lung tissue (*23*). Similarly, lungs of small experimental animals can be prepared by vascular perfusion so that the tissue is evenly expanded and optimally fixed for light and electron microscopy. The alveolar lining, airway mucous layers and deposited particulates remain unperturbed (*24*) (Figs. 1, 2 and 4).

This is accomplished according to the following protocol. Anesthetize the animal (mouse, rat, hamster) with a sublethal intraperitoneal dose of Nembutal (sodium pentobarbital or a similar fast-acting drug). When the animal is insensitive, pin it to a dissecting board and expose the trachea by dissecting carefully through the ventral neck muscles. Immediately after the trachea is exposed, it must be securely clamped or ligated to prevent further movement of air. Simultaneously open the abdominal and chest cavities so the still-beating heart and renal artery are exposed (a relatively blood-free dissection can be made by grasping the xiphisternum with "toothed" forceps, cutting the rib cage on both sides of the sternum while avoiding the intercostal arteries, reflecting the chest wall anteriorly, and pinning the xiphisternum over the animal's right shoulder). Cannulate the right ventricle and pulmonary

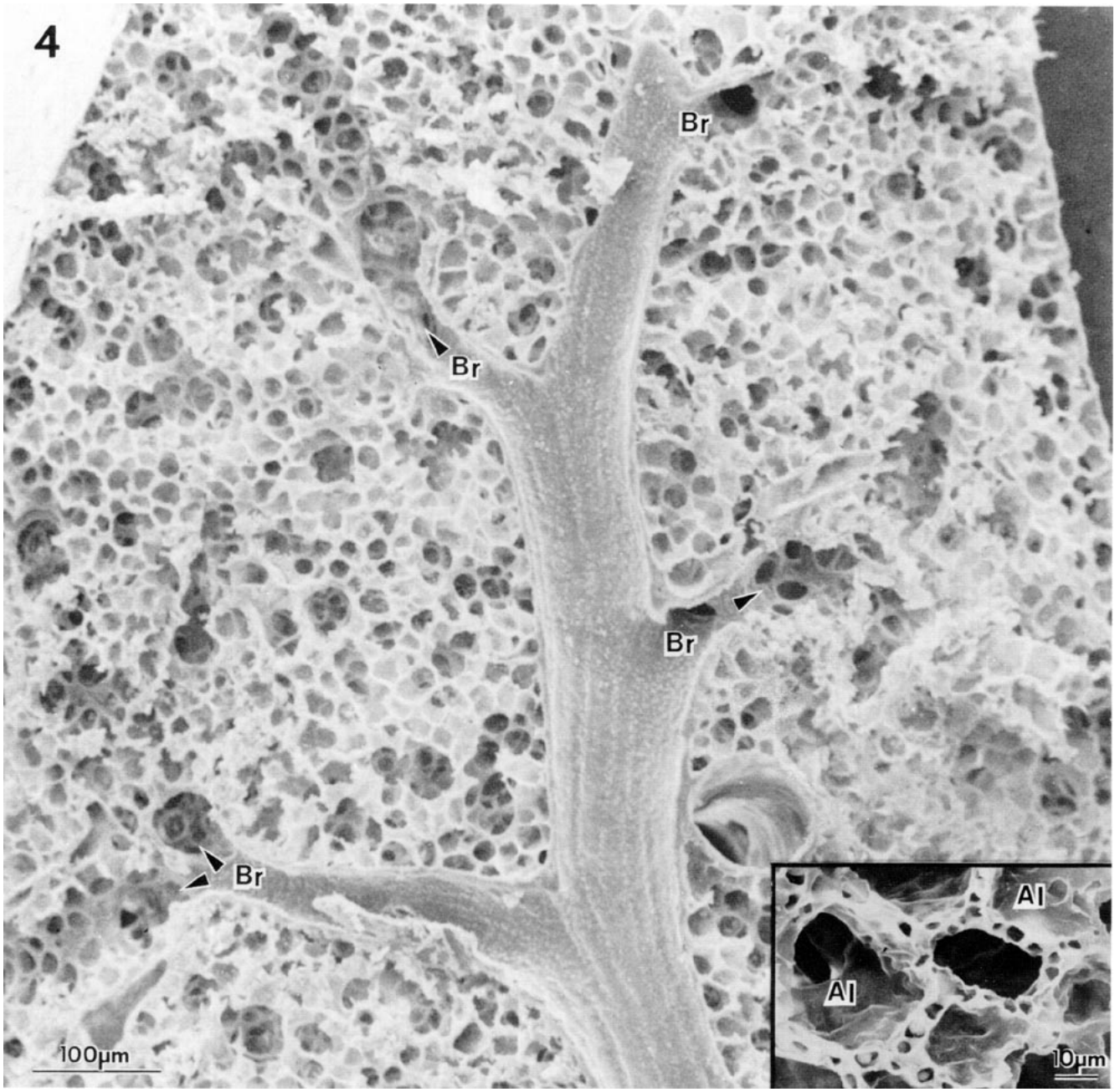

FIGURE 4. SEM of a rat lung dissection demonstrating terminal bronchioles (Br) and their alveolar ducts (arrowheads). The distal parenchyma is well expanded by vascular perfusion of fixative. The inset shows a higher magnification of alveolar spaces (Al) as well as the capillary bed which is cleared by perfusion.

artery with a 19 gauge needle extending from a reservoir of 0.80% saline located 20 to 25 cm above the animal. Begin the flow of saline and simultaneously cut the renal artery to provide an outflow tract for the perfusate which courses through the lung; continue saline perfusion for 30 sec (at this time the lungs should appear light pink to pure white), then switch to a perfusion solution of 1% buffered Karnovsky's fixative (*21*) for at least 5 min. Five to ten minutes of fixation–perfusion will make the lungs firm enough to dissect them *in toto* from the chest cavity. During dissection, the trachea must remain clamped or the lungs will collapse. After removal from the chest, the lungs should be submerged in fresh fixative for at least 8 hr before further dissection.

Separation of Particles from Tissue. Many questions regarding particle mass, size and elemental nature require the separation of inhaled particles from lung

tissue before they can be studied by electron microscopy. The most common separation techniques are tissue ashing and digestion. Ashing can be carried out at high temperature (500–600°C) in a muffle furnace or at 100°C in an oxygen plasma atmosphere (*25*). Tissue digestion usually is carried out in hot (100°C) sodium or potassium hydroxide (*18*), cold sodium hypochlorite or in proteolytic enzymes such as pronase. These techniques generally are applied to bulk tissue samples containing inorganic particulates (*26*). The ashing and digestion remove most of the surrounding biological matrix, leaving the particles unobscured. The major disadvantage of tissue removal techniques is that particles no longer have a relationship to anatomic structures and lesions. A second problem is that some particles may be partially dissolved or elementally altered. Unquestionably, some forms of inhaled particles are studied best after separation from tissue (Fig. 5).

Tissue Preparation for TEM. Cutting ultrathin sections for conventional TEM is the most tedious and technically demanding procedure of all electron microscopy methods and is well beyond the scope of this review. One must understand that the electron beam of a conventional (vs. high kV) TEM will pass through a section effectively if it is about 600 Å (or less) thick. The section should be counterstained with uranium and lead salts to enhance the shadow effect produced by electron-dense regions of the specimen (*16*). Inorganic particles are inherently electron-dense and show up well in ultra-thin sections of tissue (Fig. 3). Particles separated from tissue by ashing or digestion can be placed directly from suspension onto TEM grids coated with formvar or parlodion to provide support. Investigators have used carbon replications of particles extracted from human lung tissue to assess particle size and number (*19*).

Scanning Electron Microscopy (SEM)

A practical SEM was first available commercially in 1965. In the 1970s, investigator's recognized the potential of the SEM for diagnosing and studying lung disease (*5,27–29*) as well as for characterizing normal pulmonary anatomy (*23,30,31*). To be an effective diagnostic and investigative tool for particle-related lung disease, the SEM must be equipped with an X-ray analytical system and backscattered electron imaging capabilities (see below). The basic SEM provides an image with great depth of focus over a wide range of useful magnifications (e.g., 10× –20,000×) (Figs. 1, 2, 4 and 5). This is accomplished by passing an electron beam (from a tungsten filament as in TEM) of small diameter (~0.1 μm) through "scanning coils" which control and scan the beam in a "raster" pattern across the surface of the specimen. When the beam strikes the specimen, low energy "secondary electrons" are emitted from its atomic framework. The carbon and hydrogen molecules of biological tissue are poor sources of secondary electrons. Thus, it is necessary to coat the specimen surface with a thin (~ 250 Å) of gold, gold-palladium or other heavy metal whose atoms will provide a rich source of secondary electrons. These low energy secondary electrons are attracted to a positively charged (+10 kV) scintillator which directs the electron energy to a photomultiplier tube, which, in turn, sends the energy to a cathode ray tube upon which is recreated the electron pattern detected on the specimen surface. This reproduction appears on a phosphorescent screen for routine viewing and simultaneously on a nonphosphor screen for picture taking. Details of image formation and reproduction can be found in several sources (*17*).

Tissue Preparation for SEM. Lung tissue or in-

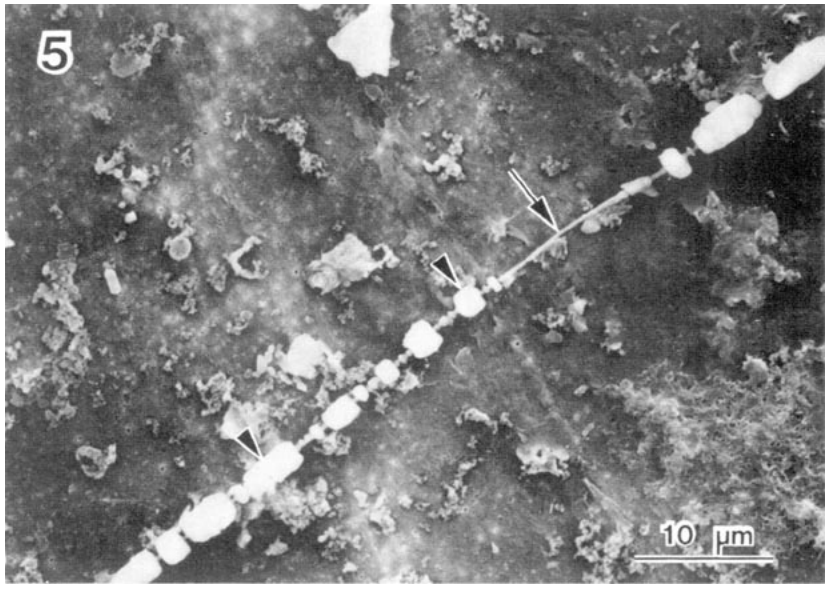

FIGURE 5. SEM of an asbestos body recovered by hypochlorite digestion from the lung of an asbestos worker. The "body" shows a thin asbestos core (arrow) surrounded by lumps of proteinaceous iron (arrowheads).

haled particles can be prepared for SEM precisely as described above for TEM. The major difference is that whole blocks of tissue rather than ultra-thin sections are studied by SEM. For example, blocks of tissue dissected to reveal conducting airways and their bifurcating ducts can be visualized on a block surface (Fig. 4). Small particulates then can be visualized at varying magnifications on the respiratory surface of vascular perfused tissues (Figs. 1 and 2). Bulk samples of tissue must be dehydrated before being placed in the vacuum of the SEM. To accomplish this while maintaining the lifelike quality of the cells, it is necessary to "critical-point-dry" the blocks of tissue. Critical-point-drying (CPD) can be carried out in a variety of commercially available pieces of equipment (*32*). The process involves first dehydrating tissue from the original aqueous fixative through a graded series of ethyl alcohols to 100% EtOH. The specimen then is placed in a CPD apparatus where tissues are immersed in liquid carbon dioxide which replaces the alcohol. After all the alcohol is removed, the liquid CO_2 in and around the tissue is changed to a gas by heating the specimen chamber. The heat causes the CO_2 to pass through its "critical" temperature ($\sim$ 30°C) and pressure (μ 1100 psi). The CO_2 gas then is slowly (20 min) bled from the chamber and simultaneously from the tissue, thus leaving the specimen dehydrated, but having bypassed the deleterious effects of surface tension distortion which occurs during dehydration from aqueous media. The tissue blocks then are placed on a solid substrate appropriate for the SEM specimen chamber and coated with a thin ($\sim$ 250 Å) layer of gold or gold-palladium as discussed above.

Inorganic particles separated from the tissue by ashing or digestion (as described under TEM) can simply be placed on a carbon substrate and viewed by SEM (Fig. 6) with no further preparation. Particles can be metal-coated to increase the resolution potential, but this could confuse X-ray analytical data (see below).

Backscattered Electron Imaging (BEI), X-Ray Energy Spectrometry (XES) and Scanning Transmission Electron Microscopy (STEM). When an electron beam interacts with tissue, a variety of signals emanates from the sample. Low energy secondary electrons used to form secondary images (Figs. 1 and 2) have been discussed above. In addition, high energy, or "backscattered," electrons are produced when the original electron beam rebounds from within the tissue matrix. The higher the atomic number of a material, the more often it will yield backscattered electrons. Consequently, dense inorganic particles in a biologic matrix of carbon and hydrogen atoms will yield a relatively high number of backscattered electrons. Scanning and transmission EMs can be equipped with detectors which send the energy from backscattered electrons to an image translation system. The images are extremely useful for determining the distribution and size of particulates in human and animal lung tissue (Figs. 1 and 7) (*5,33–35*).

X-rays are an additional form of energy resulting from electron beam penetration into tissue and particles. X-rays are produced when accelerated electrons from the primary electron beam collide with and displace orbiting electrons in the atomic framework of the specimen. As the displaced electrons return to their original orbits, X-rays are produced (*36*). The energies of these X-rays are specific for the elements from which

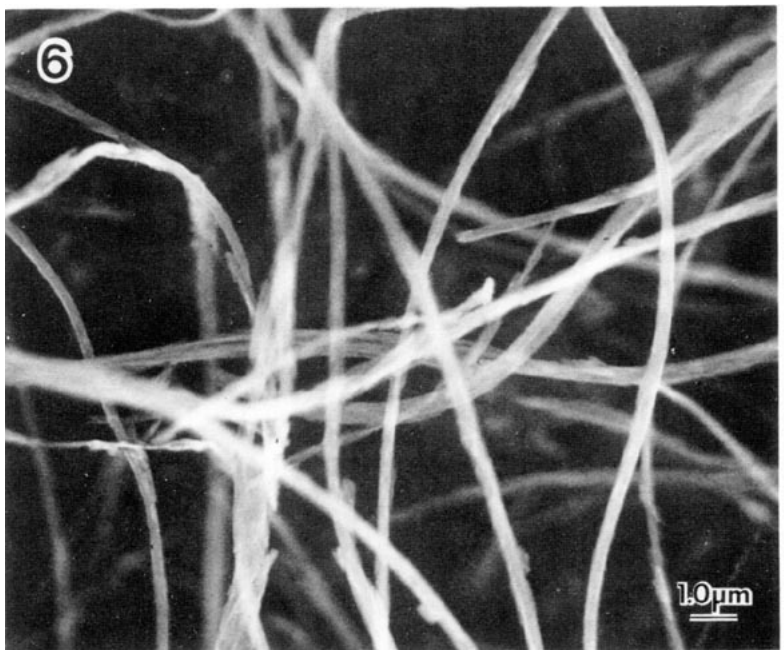

FIGURE 6. SEM demonstrates the slender, curly nature of chrysotile asbestos.

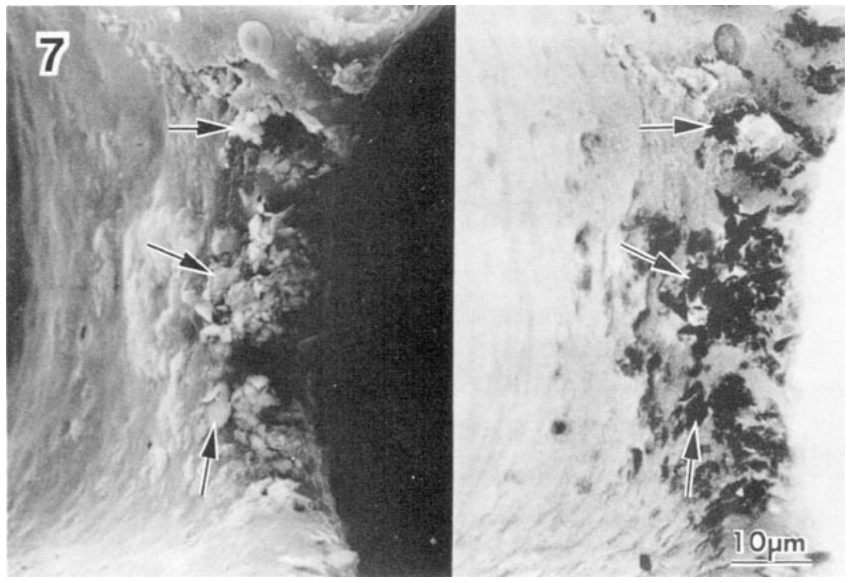

FIGURE 7. SEM (left) shows large numbers of inhaled crystalline silica particles (arrows) at a bronchiolar bifurcation in the lung of a rat. BEI of the same field (right) adds considerable contrast to the particles (arrows).

they emanated. Elements from sodium through uranium can be detected rapidly and precisely by X-ray energy spectrometry (XES). The X-rays are collected through a thin beryllium window which extends into the TEM or SEM column. The characteristic X-ray energies are sorted out into specific elemental windows on a cathode ray tube (Fig. 8). In addition to this visual spectrum, the numbers of X-rays detected per unit time can be collected for elements of choice, thus providing numerical data for semiquantitative analysis (*27,37*).

The best instrumentation for studying inhaled particles is a combination of scanning and transmission electron microscopes equipped with backscattered electron and X-ray energy detectors. This so-called analytical scanning transmission electron microscope (STEM) provides the high accelerating potential and resolution of a transmission EM, the depth of focus and large specimen accommodation of the SEM as well as the ability to determine the distribution and elemental content of inhaled particles by BEI and XES. Thicker ultramicrotomy sections (up to 1000 Å) can be utilized in a STEM because a highly energized "scanning" electron beam is produced with high accelerating potentials. This provides excellent resolution of intracellular compartments and any inorganic particles contained therein. Simultaneously, the elemental nature of these particles can be determined *in situ* (*37*).

Electron Microscopy as a Diagnostic Method

Both TEM and SEM have been used as diagnostic tools in a variety of human diseases (*5,38,39*). Here we will consider current applications of the methods in

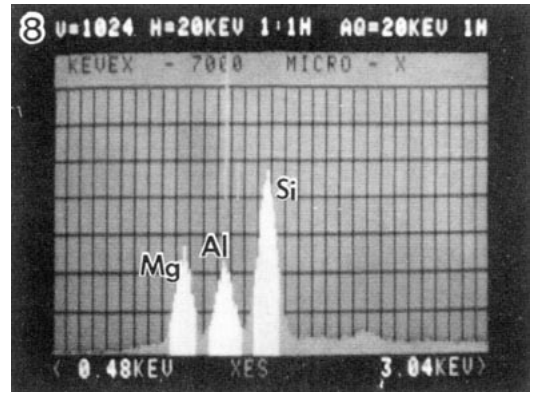

FIGURE 8. A particle separated from the lung and analyzed by X-ray energy spectrometry exhibits clear peaks for magnesium (Mg), aluminum (Al), and silicon (Si).

determining the etiology of dust-related lung disease. Certainly, dust exposure and associated disease are best understood if the inhaled agent is clearly characterized in regard to its size and mineralogical nature (*40*). One of the major difficulties in diagnosing human disease is that in occupationally exposed individuals, inhaled dust may be comprised of varied components (*5*). For example, the lungs of cigarette smokers contain increased numbers of platelike aluminum silicate crystals (i.e., the clay mineral kaolinite) (*18*). If an individual is exposed to other platy particles, such as the magnesium silicates comprising "talc," it may be difficult to determine which of the inclusions has actually incited a fibrotic response inasmuch as it has been shown that both minerals can be fibrogenic in human lungs (*1*). Another common example of mixed dust exposure can occur when an individual is exposed for several years to

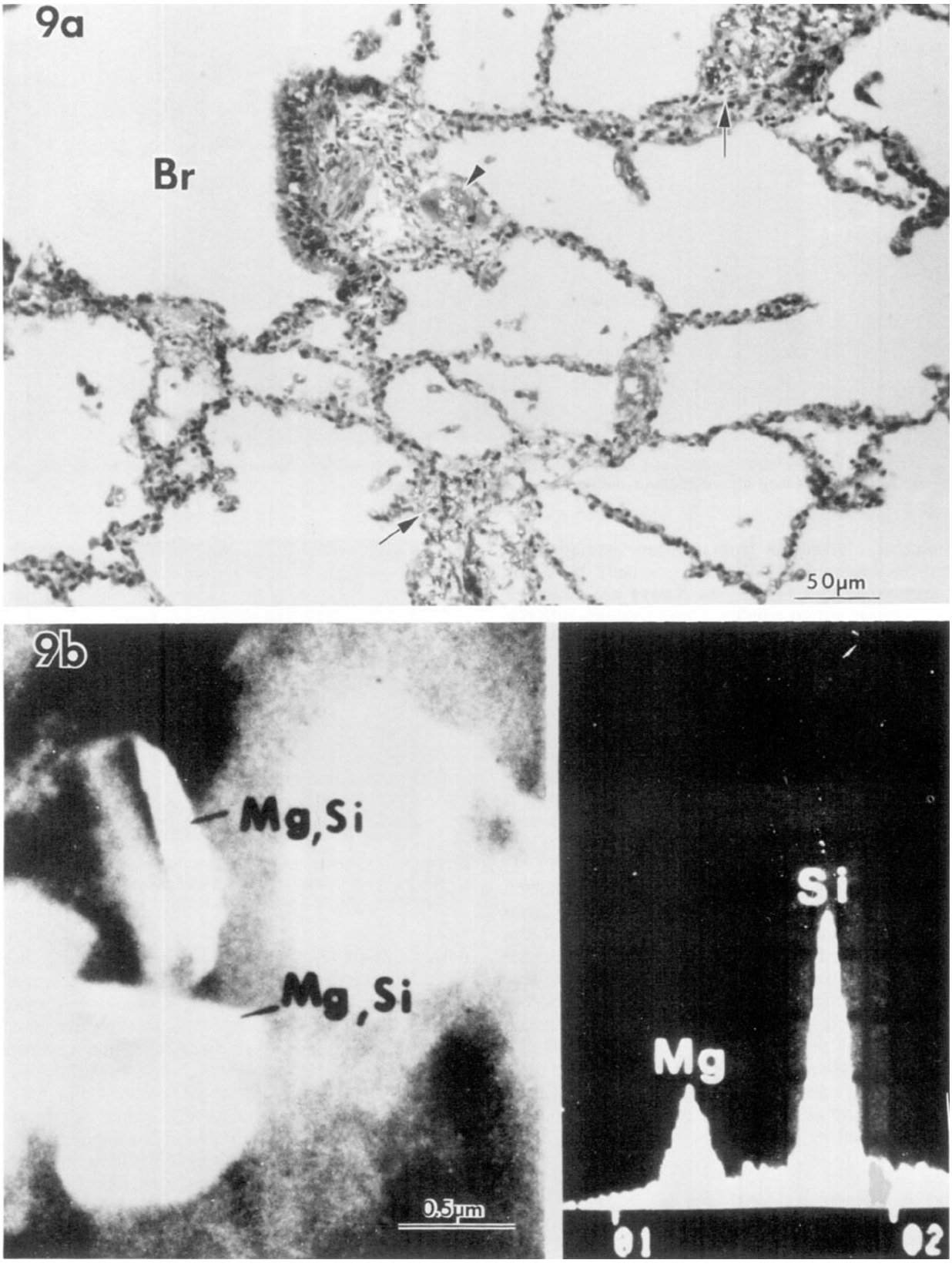

FIGURE 9. (*a*) Polarized light micrograph of lung tissue from an individual occupationally exposed to talc. A multinucleate giant cell (arrowhead) adjacent to a terminal bronchiole (Br) contains birefringent crystals. Surrounding interstitial tissues also contain numerous crystalline particles (arrows). (*b*) A backscattered electron image of a small region of tissue from the lung seen in Figure 9*a* shows several platy particles which contain magnesium and silicon at a ratio of about 0.3, characteristic of talc.

one variety of mineral dust and then changes jobs to a site where he is exposed to a different mineral. A third diagnostic problem can arise when a worker is exposed to a dust comprised of several mineral species. Coal miners, gold and hematite miners are examples. Often, the problem is insurmountable and no definitive diagnosis can be made. On the other hand, approaching selected cases with electron microscopic techniques often can yield useful information. Several examples of this are illustrated below.

Case 1: A 30-year-old man was killed accidentally in a mining mishap. A routine autopsy was performed and histopathologic review of the lungs revealed extensive interstitial thickening associated with large numbers of birefringent particulates (Fig. 9). In view of the individual's young age and limited exposure in a talc mine, a question was raised concerning whether or not the diffuse lung lesions were associated with talc or some other inhaled mineral. Thus, several paraffin-embedded histologic sections were deparaffinized in xylene as previously described (*28*). Examination of the tissue by scanning electron microscopy and X-ray energy spectrometry revealed large numbers of small platelike particles scattered through the interstitium. Almost without exception, the particles were composed of only magnesium and silicon (Fig. 9). Talc is not considered to be a highly fibrogenic dust in an occupational setting, although exposure to talc has produced pneumoconiotic lesions (*41*). The studies carried out here by SEM and XES show a clear association of talc particles with interstitial lesions in the lungs of a young, occupationally exposed individual.

Case 2: Four individuals were exposed simultaneously to an abrasive dust used for sandblasting tombstones (*42*). All had abnormal chest X-rays, were short of breath and seemed to have rapidly progressing symptoms of interstitial lung disease. Lung tissue was procured at autopsy from three of the individuals. Since all the workers were exposed to silica for a short duration (i.e., months) (*42*), the question of etiology of the lung lesions remained prominent. Histopathology demonstrated a diffuse interstitial fibrogenesis and focal fibrotic nodules. Tissue sections were deparaffinized and studied by SEM and XES. Numerous particulates were scattered within the connective tissue and yielded clear silicon peaks (Fig. 10). All tissues studied contained these particulates, strongly suggesting that the fibrotic process was caused by inhalation of large volumes of silica dust. Silica (silicon dioxide) is known to be highly fibrogenic when inhaled in an occupational setting and under experimental conditions (*1,43*).

Case 3: A 55-year-old-man had worked for many years as a heating duct insulator where it was suspected that he was exposed to asbestos. This individual had progressive, debilitating interstitial lung disease which led to his death. Lung tissue studied at autopsy revealed severe interstitial fibrosis. To determine whether or not the individual's family was eligible for workman's compensation, it was necessary to establish if significant numbers of asbestos fibers were present in the lung. Thus, tissue was digested in hypochlorite (as described above) and the inorganic residue was studied by SEM and XES. Asbestos bodies (i.e., iron-protein

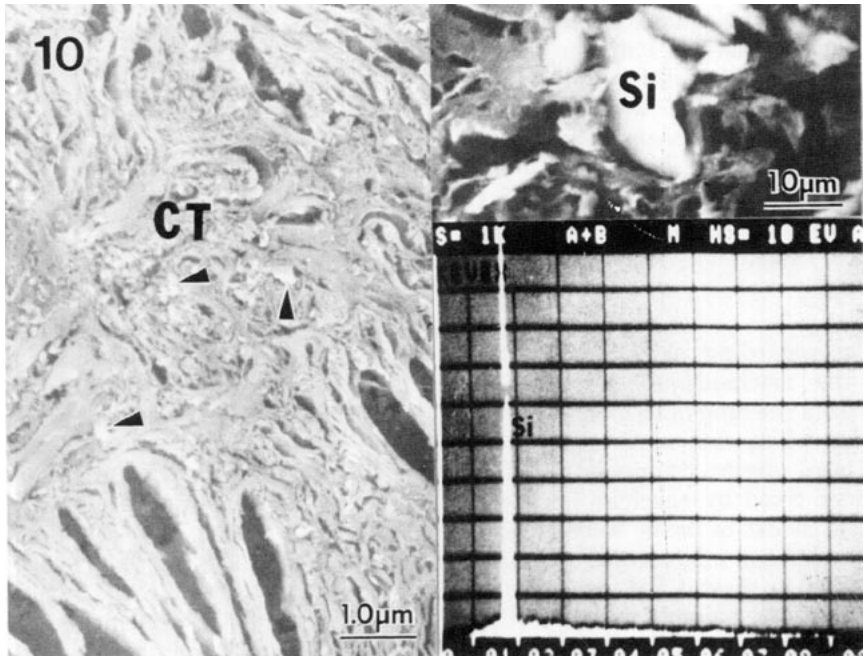

FIGURE 10. A silicotic nodule (left) prepared for SEM by deparaffinization of human autopsy lung tissue. Numerous particulates (arrowheads) are scattered through the connective tissue. X-ray energy spectrometry showed that these particles contained silicon (Si) alone.

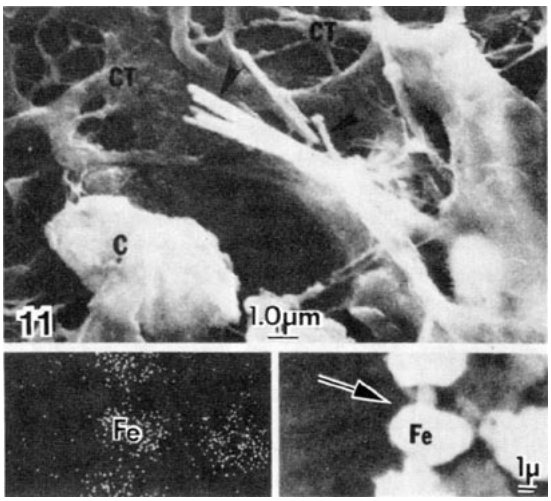

FIGURE 11. SEM shows small asbestos fibrils (arrowheads) in lung tissue from an occupationally exposed individual. This same tissue contained larger asbestos bodies (arrow), and the X-ray dot mapping technique demonstrated the presence of iron (Fe) coating portions of a fiber.

coated asbestos fibers) were readily seen by this technique (Fig. 5). Deparaffinized sections also demonstrated numerous small asbestos fibrils embedded in the tissue (Fig. 11). These techniques yielded sufficient evidence of significant exposure to amosite asbestos.

Electron Microscopy in Experimental Pneumoconiosis

It has become increasingly clear that inhaling silica and asbestos causes lung disease (*2,43*). Despite this understanding, very little is known about the basic mechanisms of dust-inhalation disease. Patterns of dust deposition and pathogenesis of the initial lung lesions are important factors about which we have little information. Studies with electron beam instruments recently have added new information. Several examples of such work ongoing in our laboratory are described below.

Silica Inhalation

Many questions exist regarding patterns of initial dust deposition and the mechanisms which subsequently clear particles from the lung (*8,24*). To approach some of these questions, white rats were exposed for 3 hr to 100 mg/m^3 of pure quartz. Immediately after exposure, the lungs were fixed by vascular perfusion and removed *in toto* (*34*). Blocks of tissue were critical-point-dried for scanning electron microscopy, and adjacent tissue was embedded in plastic for transmission electron microscopy. Additional animals were anesthetized and the lungs lavaged with saline to recover pulmonary macrophages. These cells were allowed to adhere to coverslips as a monolayer (*44*).

Backscatter electron imaging was used to demonstrate the number of silica particles on alveolar duct surfaces (Fig. 7). We found that the number of particles per micon-squared of alveolar duct surface was reduced significantly 24 hr after the original 3-hr exposure (*34,45*). In addition, we learned that the macrophages lavaged from exposed animals contained varying numbers of silica particles. X-ray energy spectrometry in concert with SEM was used to determine the percentage of lavaged macrophages which contained silica. Interestingly enough, the percentage of these silica-containing cells increased to about 60% over the first 24 hr after exposure and remained close to this level through the following 4 weeks. Transmission electron microscopic studies of thin-sectioned lung tissue from the silica-exposed animals showed that macrophages on alveolar surfaces also contained inhaled silica particles (Fig. 12). As correlates with the findings in the lavaged cells, more of these macrophages *in situ* contained silica 24 hr after exposure than did macrophages observed immediately after exposure. This suggests that lavaged macrophages are representative of the phagocytes which populate the alveolar spaces (*45*), an issue which has been raised by several investigators (*46,47*). Thus, in silica-exposed animals, several electron beam techniques have allowed us to approach a variety of basic questions concerning dust deposition and clearance.

Asbestos Inhalation

Lung disease caused by inhalation of asbestos fibers is a well-known and well-characterized affliction commonly found in occupationally exposed individuals (*2*). However, very little is known about the basic mechanisms through which asbestos causes fibrotic and neoplastic lung disease. We have pursued several fundamental questions regarding particle deposition and development of an initial pulmonary lesion in an animal model of asbestosis (*24*). White rats were exposed for 1 hr to ~ 10 mg/m^3 of chrysotile asbestos aerosolized in an inhalation chamber. Animals were sacrificed immediately (within 4.5 min) at the cessation of exposure and at 5 hr and 24 hr and at 4, 8 and 30 days after exposure. The first new information acquired concerned the deposition pattern of inhaled chrysotile fibers. It was surprising to find that immediately after exposure, asbestos fibers which were small enough to pass through the conducting airways deposited primarily at the bifurcations of alveolar ducts (Fig. 2). Fibers rarely were found in alveolar spaces or on alveolar duct surfaces other than at bifurcations. A semiquantitative SEM method was used to determine the comparative degree of asbestos deposition on alveolar duct bifurcations (*24,48*). This method showed that the majority of fibers deposited on the alveolar duct bifurcations closest to terminal bronchioles. The farther an alveolar duct bifurcation was from its terminal bronchiole, the less asbestos was observed (*48*). Preliminary data suggest that the diameter of these alveolar duct fibers

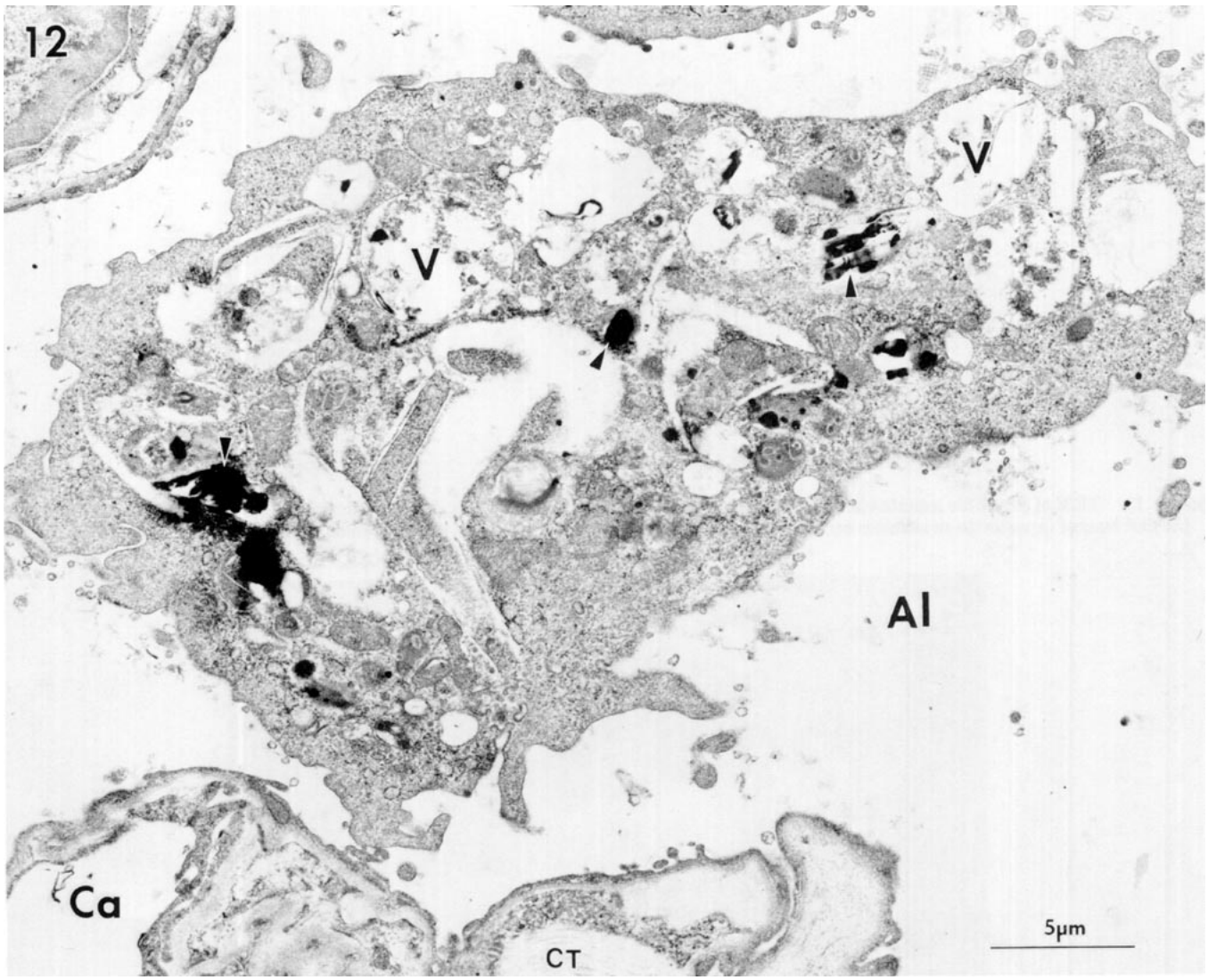

FIGURE 12. TEM illustrates crystalline silica (arrowheads) in a macrophage found in an alveolus (Al). Intracellular vacuoles (V) signal toxic effects of the phagocytized silica. A nearby capillary (Ca) and connective tissue (CT) are seen.

averages ~0.20 μm. Studies are ongoing to determine whether or not the varying diameters of these small fibers dictate their depth of penetration into the alveolar ducts.

Scanning and transmission electron microscopy showed that many of the small asbestos fibers which impacted on alveolar duct bifurcations were taken up by underlying epithelial cells (Fig. 13). Other fibers were phagocytized by alveolar macrophages (Fig. 3). A significant advance in our understanding of alveolar clearance mechanisms was made when we found that asbestos particles taken up by epithelial cells passed through basement membranes and into interstitial connective tissue (*24,49*).

A combination of light and electron microscopy demonstrated the anatomic regions where the pulmonary reaction to asbestos was initiated. Interestingly enough, the initial lesion was characterized as an accumulation of macrophages at precisely the same regions that the asbestos first landed (*50*), i.e., at the bifurcations of alveolar ducts (Fig. 14). This correlates with the findings of others who have established that the prominent early lesions of asbestosis in animals and man are located at the junctions of bronchioles and alveolar ducts (*6*).

Several investigations have centered upon the elemental nature of asbestos and its significance in causing cytotoxicity (*51,52*). Using SEM and TEM in concert with X-ray energy spectrometry (XES), we have studied some elemental characteristics of chrysotile asbestos *in vitro* and *in vivo* after inhalation (*37*). The magnesium content of the fibers was altered *in vitro* simply by treating the fibers with 1 N HCl. This alteration in elemental content was measured by analyzing the changes of Mg to Si ratios in individual asbestos fibers (*37*). XES demonstrated that inhaled chrysotile

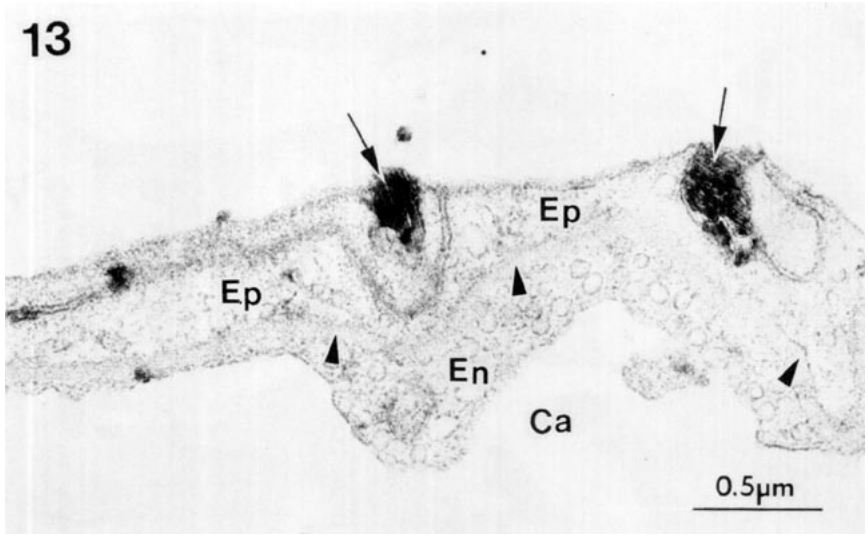

FIGURE 13. TEM of chrysotile asbestos (arrows) within the Type I epithelium (Ep) of a rat. This phenomenon of epithelial uptake occurs during the first hour of exposure to an asbestos aerosol. The basement membrane (arrowheads), capillary endothelium (En) and lumen (Ca) are seen.

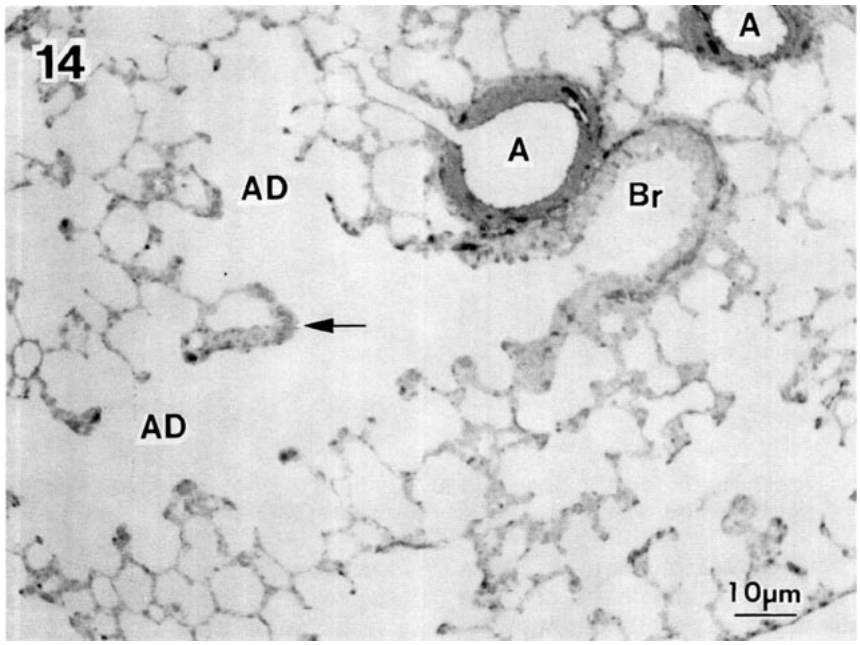

FIGURE 14. Light micrograph of plastic-embedded lung tissue from a rat 24 hr after a 1-hr exposure to chrysotile asbestos. The first alveolar duct bifurcation (arrow) is prominent because increased numbers of alveolar macrophages have migrated to this region (see Fig. 3) where the asbestos initially was deposited. Terminal bronchiole (Br), alveolar duct (AD), arteriole (A).

asbestos also was changed in elemental character after inhalation. Further studies will be necessary to determine whether or not alterations in the elemental content of asbestos play any role in the cytotoxic potential of the fibers *in situ* after inhalation.

Summary

Scanning and transmission electron microscopy in concert with X-ray energy spectrometry are powerful tools for enhancing our knowledge of dust-related lung disease. The excellent resolution afforded by current state-of-the-art instrumentation allows the investigator to make a variety of useful observations, e.g., precise physical and elemental characteristics of inhaled particles, the initial deposition sites of the particles and subsequent clearance pathways, and ultrastructural alterations of cells involved in pulmonary clearance and associations of these cells with inhaled particles of specific elemental composition.

REFERENCES

1. Parkes, W. R. Occupational Lung Disorders. Butterworth and Co., London, 1974.
2. Selikoff, I. J., and Lee, D. H. Asbestos and Disease. Academic Press, New York, 1978.
3. Ziskind, M., Jones, R. N. and Weill, H. Silicosis: state of the art. Am. Rev. Respir. Dis. 113: 643–658 (1976).
4. Fruchter, J. S., Robertson, D. E., Evans, J. C., et al. Mount St. Helens ash from the 18 May 1980 eruption: chemical, physical, mineralogical, and biological properties. Science 209: 1116–1117 (1980).
5. Abraham, J. L. Recent advances in pneumoconisis: the pathologists' role in etiologic diagnosis. In: Lung, Structure, Function and Disease (W. M. Thurlbeck and M. R. Abell, Eds.), Williams and Wilkins Co., Baltimore, 1978, pp. 96–137.
6. Wagner, J. C. Berry, G., Skidmore, J. W. and Timbrell, V. The effects of the inhalation of asbestos in rats. Brit. J. Cancer 29: 252–269 (1974).
7. Zaidi, S. H. Experimental Pneumoconiosis. Johns Hopkins Press, Baltimore, 1969.
8. Brain, J. D., and Valberg, P. A. Deposition of aerosol in the respiratory tract. Am. Rev. Respir. Dis. 120: 1325–1373 (1979).
9. Lippman, M., and Albert, R. E. The effect of particle size on the regional distribution of inhaled aerosols in the human respiratory tract. Am. Ind. Hyg. Assoc. J. 30: 257–270 (1969).
10. Raabe, O. G., Yeh, H. C., Newton, G. J., Phalen, R. F., and Velasquez, D. J. Deposition of inhaled monodisperse aerosols in small rodents. In: Inhaled Particles and Vapors (W. H. Walton, Ed.), Pergamon Press, New York, 1977, pp. 3–21).
11. Timbrell, V. The inhalation of fibrous dusts. Ann. N.Y. Acad. Sci. 133: 255–273 (1965).
12. Green, G. M., Jakab, G. J., Low, R. B., and Davis, G. S. Defense mechanisms of the respiratory membrane. Am. Rev. Respir. Dis. 115: 479–514 (1977).
13. Kilburn, K. H. An hypothesis for pulmonary clearance and its implications. Am. Rev. Respir. Dis. 98: 449–458 (1968).
14. Lauweryns, J. M., and Baert, J. H. Alveolar clearance and the role of pulmonary lymphatics. Am. Rev. Respir. Dis. 115: 625–683 (1977).
15. Wischnitzer, S. Introduction to Electron Microscopy. Pergamon Press, New York, 1962.
16. Pease, D. C. Histological Techniques for Electron Microscopy. Academic Press, New York, 1964.
17. Johari, O. (Ed.) Scanning Electron Microscopy. IIT Research Inst., Chicago, 1972–1977; SEM Inc., Chicago, 1978–1981.
18. Brody, A. R., and Craighead, J. E. Cytoplasmic inclusions in pulmonary macrophages of cigarette smokers. Lab. Invest. 32: 125–137 (1975).
19. Pooley, F. E. Electron microscope characteristics of inhaled chrysotile asbestos fibre. Brit. J. Ind. Med. 29: 146–153 (1972).
20. Ruttner, J. R., Spycher, M. A., and Sticher, H. The detection of etiologic agents in interstitial pulmonary fibrosis. Human Pathol. 4: 497–508 (1973).
21. Karnovsky, M. J. A formaldehyde-glutaraldehyde mixture of high osmolality for use in electron microscopy. J. Cell Biol. 27: 137–138 (1965).
22. Hill, L. H., and Plopper, C. G. Use of large block embedding for correlated LM, TEM, and SEM characterization of pulmonary airways of known anatomic location. Proc. Southeast Electr. Microsc. Soc. 2: 24–26 (1979).
23. Brody, A. R., and Craighead, J. E. Preparation of human lung biopsy specimens by perfusion-fixation. Am. Rev. Respir. Dis. 112: 645–650 (1975).
24. Brody, A. R., Hill, L. H., Adkins, B., and O'Connor, R. W. Chrysotile asbestos inhalation in rats: deposition pattern, reaction of the alveolar epithelium and pulmonary macrophages. Am. Rev. Respir. Dis. 123: 670–679 (1981).
25. Thomas, R. S., and Hollahan, J. R. Use of chemically reactive gas plasmas in preparing specimens for scanning electron microscopy and electron probe microanalysis. In: Scanning Electron Microscopy (O. Johari, Ed.), IIT Research Inst., Chicago, 1974, pp. 83–90.
26. Johari, O., and De Nee, P. B. Handling, mounting and examination of particles for scanning electron microscopy. In: Scanning Electron Microscopy (O. Johari, Ed.), IIT Research Inst., Chicago, 1972, pp. 249–256.
27. Brody, A. R., Dwyer, D. M., Vallyathan, N. V. Visco, G. P., and Craighead, J. E. The elemental content of granulomata: studies of pulmonary sarcoidosis and hypersensitivity pneumonitis. In: Scanning Electron Microscopy (O. Johari and R. P. Becker, Eds.), ITT Research Inst., Chicago, 1977, pp. 129–136.
28. Brody, A. R., Vallyathan, N. V., and Craighead, J. E. Distribution and elemental analysis of inorganic particles in pulmonary tissue. In: Scanning Electron Microscopy (O. Johari, Ed.), IIT Research Inst., Chicago, 1976, pp. 477–484.
29. DeNee, P. B., Abraham, J. L., and Gelderman, A. H. Methods for a SEM study of coal workers pneumoconiosis. In: Scanning Electron Microscopy (O. Johari, Ed.), IIT Research Inst., Chicago, 1973, pp. 411–418.
30. Wang, N. S., and Thurlbeck, W. M. Scanning electron microscopy of the lung. Human Pathol. 1: 288–297 (1970).
31. Kuhn, C., and Finke, E. D. The topography of the pulmonary alveolus: scanning electron microscopy using different fixations. J. Ultrastr. Res. 38: 161–173 (1972).
32. Nowell, J. A., Pangborn, J., and Tyler, W. S. Stabilization and replication of soft tubular and alveolar systems. In: Scanning Electron Microscopy (O. Johari, Ed.), IIT Research Inst., Chicago, 1972, pp. 305–312.
33. Becker, R. P., and Sogard, M. Visualization of subsurface structures in cells and tissues by backscattered electron imaging. In: Scanning Electron Microscopy (O. Johari and R. P. Becker, Eds.), SEM Inc., Chicago, 1979, pp. 835–842.
34. Brody, A. R., Roe, M. W., Evans, J. N., and Davis, G. S. Use of backscattered electron imaging to quantify the distribution of inhaled crystalline silica. In: Scanning Electron Microscopy (O. Johari and R. P. Becker, Eds.), SEM Inc., Chicago, 1980, pp. 301–306.
35. DeNee, P. B., and Abraham, J. L. Backscattered electron imaging (application of atomic number contract). In: Principles and Techniques of Scanning Electron Microscopy, Vol. 5 (M. A. Hayat, Ed.), Van Nostrand-Reinhold, New York, 1976, pp. 144–165.
36. Erasmus, D. A. Electron Probe Microanalysis. Chapman and Hall, London, 1978.
37. Brody, A. R. Elemental content of chrysotile asbestos: Mg/Si ratios *in vitro* and *in situ* after fiber inhalation. J. Environ. Pathol. Toxicol. In press.
38. Carter, H. W. Clinical applications of scanning electron microscopy in North America with emphasis on SEM's role in comparative microscopy. In: Scanning Electron Microscopy (O. Johari, Ed.), SEM Inc., Chicago, 1980, pp. 115–120.
39. Vallyathan, N. V., Green, F. H., and Craighead, J. E. Recent advances in the study of mineral pneumoconiosis. In: Pathology Annual, Part 2 (S. C. Sommers and P. P. Rosen, Eds.), Appleton-Century-Crofts, 1980, pp. 77–104.
40. Brody, A. R., and DeNee, P. B. Biological activity of inhaled inorganic particles. In: CRC Uniscience Series on Environmental Control (C. Straub, Ed.), CRC Press, Boca Raton, FL, 1981, pp. 277–299.
41. Vallyathan, N. V., and Craighead, J. E. Pulmonary pathology in workers exposed to nonasbestiform talc. Human Pathol. 12: 28–35 (1981).
42. Suratt, P. M., Winn, W. C., and Brody, A. R. Acute silicosis in tombstone sandblasters Am. Rev. Respir. Dis. 115: 521–528 (1977).
43. Spencer, H. Pathology of the Lung. W. B. Saunders Co., Philadelphia, 1977.
44. Davis, G. S., Adler, K. B., and Brody, A. R. Changes in the surface morphology of human alveolar macrophages induced by tobacco and marijuana smoking. Exptl. Lung Res. 1: 281–288 (1980).
45. Brody, A. R., Roe, M. W., Evans, J. N., and Davis, G. S.

Deposition and translocation of inhaled silica in rats: quantification of particle distribution, macrophage participation and function. Lab. Invest. 47: 533–542 (1982).
46. Brain, J. D., Godleski, J. J., and Sorokin, S. P. Quantification, origin, and fate of pulmonary macrophages. In: Respiratory Defense Mechanisms (J. D. Brain, D. F. Proctor, and L. M. Reid, Eds.), Marcel Dekker, New York, 1977, pp. 849–892.
47. Davis, G. S., Brody, A. R., and Craighead, J. E. Analysis of airspace and interstitial mononuclear cell populations in human diffuse interstitial lung disease. Am. Rev. Respir. Dis. 118: 7–18 (1978).
48. Brody, A. R., and Roe, M. W. Deposition pattern of inorganic particles at the alveolar level in the lungs of rats and mice. Am. Rev. Respir. Dis. 128: 724–729 (1983).
49. Brody, A. R., and Hill, L. H. Interstitial accumulation of inhaled chrysotile asbestos fibers and consequent formation of microcalcifications. Am. J. Pathol. 109: 107–116 (1982).
50. Warheit, D. B., Chang, L. Y., Hill, L. H., Hook, G. E. R., Crapo, J. D., and Brody, A. R. Pulmonary macrophage accumulation and asbestos-induced lesions at sites of fiber deposition. Am. Rev. Respir. Dis. 129: 301–310 (1984).
51. Harrington, J. S., Allison, A. C., and Badami, D. B. Mineral fibers: chemical, physicochemical and biological properties. Adv. Chemother. Pharmacol. 12: 291–402 (1975).
52. Morgan, A., Davies, P., Wagner, J. C., Berry, G., and Holmes, A. The biological effects of magnesium leached chrysotile asbestos. Brit. J. Exptl. Pathol. 58: 465–476 (1977).